

# LANGMUIR

Subscriber access provided by Kaohsiung Medical University

Interfaces: Adsorption, Reactions, Films, Forces, Measurement Techniques, Charge Transfer, Electrochemistry, Electrocatalysis, Energy Production and Storage

## Electronic Structure of a Self-Assembled Monolayer with Two Surface Anchors: 6-Mercaptopurine on Au(111)

Cynthia Carolina Fernandez, Evangelina Pensa, Pilar Carro,  
Roberto Carlos Salvarezza, and Federico José Williams

*Langmuir*, **Just Accepted Manuscript** • DOI: 10.1021/acs.langmuir.8b00807 • Publication Date (Web): 01 May 2018

Downloaded from <http://pubs.acs.org> on May 4, 2018

### Just Accepted

“Just Accepted” manuscripts have been peer-reviewed and accepted for publication. They are posted online prior to technical editing, formatting for publication and author proofing. The American Chemical Society provides “Just Accepted” as a service to the research community to expedite the dissemination of scientific material as soon as possible after acceptance. “Just Accepted” manuscripts appear in full in PDF format accompanied by an HTML abstract. “Just Accepted” manuscripts have been fully peer reviewed, but should not be considered the official version of record. They are citable by the Digital Object Identifier (DOI®). “Just Accepted” is an optional service offered to authors. Therefore, the “Just Accepted” Web site may not include all articles that will be published in the journal. After a manuscript is technically edited and formatted, it will be removed from the “Just Accepted” Web site and published as an ASAP article. Note that technical editing may introduce minor changes to the manuscript text and/or graphics which could affect content, and all legal disclaimers and ethical guidelines that apply to the journal pertain. ACS cannot be held responsible for errors or consequences arising from the use of information contained in these “Just Accepted” manuscripts.



ACS Publications

is published by the American Chemical Society, 1155 Sixteenth Street N.W.,  
Washington, DC 20036

Published by American Chemical Society. Copyright © American Chemical Society.  
However, no copyright claim is made to original U.S. Government works, or works  
produced by employees of any Commonwealth realm Crown government in the course  
of their duties.

1  
2  
3  
4  
5  
6  
7  
8  
9  
10  
11  
12  
13  
14  
15  
16  
17  
18  
19  
20  
21  
22  
23  
24  
25  
26  
27  
28  
29  
30  
31  
32  
33  
34  
35  
36  
37  
38  
39  
40  
41  
42  
43  
44  
45  
46  
47  
48  
49  
50  
51  
52  
53  
54  
55  
56  
57  
58  
59  
60

# Electronic Structure of a Self-Assembled Monolayer with Two Surface Anchors: 6-Mercaptopurine on Au(111)

*Cynthia C. Fernández<sup>a</sup>, Evangelina Pensa<sup>b</sup>, Pilar Carro<sup>c</sup>, Roberto Salvarezza<sup>b</sup>, Federico J. Williams<sup>a\*</sup>*

<sup>a</sup>Departamento de Química Inorgánica, Analítica y Química Física, Facultad de Ciencias Exactas y Naturales, INQUIMAE-CONICET, Universidad de Buenos Aires, Ciudad Universitaria, Pabellón 2, Buenos Aires C1428EHA, Argentina

<sup>b</sup>Instituto de Investigaciones Fisicoquímicas Teóricas y Aplicadas (INIFTA), Facultad de Ciencias Exactas, Universidad Nacional de La Plata, CONICET, La Plata 1900, Argentina

<sup>c</sup>Área de Química Física, Departamento de Química, Facultad de Ciencias, Universidad de La Laguna, Instituto de Materiales y Nanotecnología, Avda. Francisco Sánchez, s/n 38200-La Laguna, Tenerife, Spain

\* corresponding author e-mail: [fwilliams@qi.fcen.uba.ar](mailto:fwilliams@qi.fcen.uba.ar)

**ABSTRACT**

The electronic structure of aromatic and aliphatic thiols on Au(111) has been extensively studied in relation to possible applications in molecular electronics. In this work, the effect on the electronic structure of an additional anchor to the S–Au bond using 6-mercaptopurine as a model system has been investigated. Results from XPS, NEXAFS and DFT confirm that this molecule adsorbs on Au(111) with S–Au and iminic N–Au bonds. Combined UPS and DFT data reveal that formation of the 6MP self-assembled monolayer generates a molecular dipole perpendicular to the surface with negative charges residing at the metal/monolayer interface and positive charges at the monolayer/vacuum interface which lowers the substrate work function. STM shows two surface molecular domains: a well-ordered rectangular lattice where molecules are tilted in average  $30^\circ$  with respect to the substrate and aligned 6MP islands where molecules are standing upright. Finally, we found a new electronic state located at -1.7 eV with respect to the Fermi level that corresponds to a localized  $\pi$  molecular state while the state corresponding to the N–Au bond is hybridized with Au d electrons and stabilized at much lower energies (-3 eV).

## INTRODUCTION

Purines are heterocyclic compounds consisting of an imidazole ring fused with a pyrimidine ring. These aromatic molecules are present in diverse biological systems and take part in the core structure of guanine and adenine. One of the most important purines is 6-mercaptopurine (6MP), a synthetic nitrogen containing heterocyclic thiol that is very effective for the treatment of leukemia, autoimmune disorders and other diseases.<sup>1,2</sup>

The adsorption of 6MP on solid substrates have attracted considerable attention because some of the problems found in the pharmacological treatment could be circumvent using 6MP functionalized nanoparticles as carriers.<sup>3-5</sup> As a consequence, the structural properties of 6MP over solid surfaces were studied over the past years. 6MP chemisorbs strongly on Au surfaces after the formation of S–Au thiolate and iminic N–Au bonds, i.e. it forms a double anchor to Au substrates.<sup>6</sup> The molecule self-assembles on Au(111) single crystal surfaces lifting the substrate reconstruction.<sup>7</sup> Interestingly, these ordered structures do not contain staple moieties (RS–Au<sub>ad</sub>–SR) which are a proposed adsorption model for thiol based self-assembled monolayers (SAMs).<sup>8</sup> Chemisorption of the molecule on Au(111) yields short-range ordered two dimensional lattices whereas chemisorption on Au(001) results in long-range well-ordered SAMs.<sup>9</sup> 6MP molecules bind to silver surfaces with a tilted molecular plane,<sup>10,11</sup> whereas they adsorb with a flat lying geometry over graphene layers.<sup>12</sup> Vibrational spectroscopic measurements suggest that 6MP molecules bind on Au surfaces with the molecular plane standing upright.<sup>13</sup> Although the molecular structure of the adsorbate has been studied on different substrates, its electronic structure has only been measured on graphene surfaces using photoemission spectroscopy.<sup>12</sup> Furthermore, little is known about the electronic structure of thiol

1  
2  
3 SAMs with an additional N–Au interaction. Thus, the study of the electronic density of states of  
4  
5 6MP on Au is both relevant and interesting.  
6  
7

8  
9 In this work we present a detailed study of the valence electronic structure of 6MP self-  
10 assembled monolayers on Au(111) surfaces. New insights arise from the combination of  
11 photoemission measurements, and density functional theory (DFT) calculations. Furthermore,  
12  
13 near-edge X-ray absorption fine structure spectroscopy (NEXAFS) and scanning tunneling  
14  
15 microscopy (STM) measurements combined with DFT calculations provide a clear description of  
16  
17 the molecular adsorption geometry.  
18  
19  
20  
21  
22  
23  
24  
25  
26

## 27 **EXPERIMENTAL SECTION**

28  
29  
30 **Materials.** Photoelectron and near edge X-ray absorption fine structure spectroscopy  
31 measurements were carried out using a Au(111) single crystal (MaTecK GmbH). 6-  
32 Mercaptopurine was obtained from Sigma-Aldrich and used as received. Absolute ethanol of  
33 analytical grade was used to prepare solutions.  
34  
35  
36  
37  
38  
39

40 **Sample Preparation.** The Au(111) crystal was Ar<sup>+</sup> sputtered and annealed until no impurities  
41 are detected by XPS. Self-assembled monolayer formation was performed under ultrapure Ar  
42 atmosphere in a ultrahigh vacuum (UHV) chamber equipped with a transfer system that allows  
43 transferring the Au(111) sample between UHV and the atmospheric liquid reactor attached to the  
44 UHV chamber (described fully elsewhere).<sup>14</sup> The clean Au crystal was placed in contact with a 1  
45 mM solution of 6-mercaptopurine in ethanol at room temperature overnight. This was followed  
46  
47 by copious rinsing with ethanol and drying with an Ar stream. Afterwards the functionalized  
48  
49  
50  
51  
52  
53  
54  
55  
56  
57  
58  
59  
60

1  
2  
3 surface is transferred back to the UHV analysis chamber. Note that we tried varying the  
4  
5 molecular coverage by changing the immersion time from 30 min to 24 hours observing the  
6  
7 same coverage in all cases.  
8  
9

10  
11 **Photoelectron Spectroscopies.** X-ray Photoelectron Spectroscopy (XPS) measurements were  
12  
13 performed using an UHV chamber (base pressure  $5 \times 10^{-10}$  mbar) with a SPECS spectrometer  
14  
15 system equipped with a 150 mm mean radius hemispherical electron energy analyzer and a nine  
16  
17 channeltron detector. XP spectra were acquired at a constant pass energy of 20 eV using a  
18  
19 monochromatic Al K $\alpha$  (1486.6 eV) source operated at 15 kV and 20 mA at a detection angle of  
20  
21 20° with respect to the sample normal. Binding energies are referred to the Au 4f $_{7/2}$  emission at  
22  
23 84 eV. Ultraviolet Photoelectron Spectroscopy (UPS) spectra were acquired using a He I  
24  
25 radiation source (21.21 eV) with normal detection using a constant pass energy of 2 eV.  
26  
27 Samples were biased -10 V in order to resolve the secondary electron cut-off in the UPS spectra.  
28  
29 Work function values were determined from the width of the UPS spectra as discussed below.  
30  
31  
32  
33  
34

35 **Near Edge X-ray Absorption Fine Structure Spectroscopy (NEXAFS)** measurements were  
36  
37 carried out at the Brazilian Synchrotron Light Source (LNLS), Campinas, Brazil using the planar  
38  
39 grating monochromator (PGM) beamline for soft X-ray spectroscopy (100-1500 eV) as the  
40  
41 monochromatic photon source. Experiments were performed using the photoemission end station  
42  
43 with a base pressure of  $10^{-10}$  mbar. NEXAFS spectra were obtained by measuring the total  
44  
45 electron yield (electron current at the sample) simultaneously with a photon flux monitor  
46  
47 (electron current at a Au mesh). The final data were normalized with respect to the Au mesh  
48  
49 electron current to correct for fluctuations in the beam intensity. NEXAFS spectra were recorded  
50  
51 at 90°, 70°, 50° and 30° photon incidence angle with respect to the sample surface. All angle  
52  
53 dependent geometry effects (for example sampling a different number of surface species) are  
54  
55  
56  
57  
58  
59  
60

1  
2  
3 eliminated by normalizing the resonant intensities to the angle-independent K-edge jump in all  
4 spectra.<sup>15</sup>  
5  
6

7  
8 **Scanning Tunneling Miscroscopy.** STM imaging was done in air in the constant current  
9 mode with a Nanoscope IIIa microscope from Veeco Instruments (Santa Barbara, CA) with  
10 mechanically cut Pt-Ir tips (80:20%, Goodfellow, UK). Typical tunneling currents, bias voltages,  
11 and scan rates were 0.3 to 0.5 nA, 200-500 mV, and 1-5 Hz, respectively. Evaporated Au films  
12 on glass with (111) preferred orientation (AF 45 Berliner Glass KG, Germany) were used as  
13 substrates. After annealing for 5 min using a hydrogen flame, the Au substrates exhibit  
14 atomically smooth (111) terraces (usually 100-500 nm wide) separated by monatomic high steps.  
15  
16  
17  
18  
19  
20  
21  
22  
23  
24

25 **Computational methods.** Electronic structure calculations were performed using density  
26 functional theory (DFT) with the periodic plane-wave basis set code VASP 5.2.12.<sup>16</sup> We have  
27 followed the scheme of non-local functional proposed by Dion et al.<sup>17</sup>, vdW-DF, and the  
28 optimized Becke88 exchange functional optB88-vdW<sup>18</sup> to take into account van der Waals  
29 (vdW) interactions. The projector augmented plane wave (PAW) method has been used to  
30 represent the atomic cores with PBE potential.<sup>19</sup> The electronic wave functions were expanded in  
31 a plane-wave basis set with a 420 eV cutoff energy. Optimal grid of Monkhorst-Pack<sup>20</sup> k-points  
32  $7 \times 3 \times 1$  has been used for numerical integration in the reciprocal space of the  $\begin{pmatrix} 2 & 0 \\ 3 & 6 \end{pmatrix}$  unit cell.  
33  
34 The Au(111)-(1 $\times$ 1) substrates were represented by a five atomic layer and a vacuum of  $\sim 17$  Å  
35 that separates two successive slabs. Surface relaxation is allowed in the three uppermost Au  
36 layers of the slab and the atomic coordinates of the adsorbed species were allowed to relax  
37 without further constraints. The atomic positions were relaxed until the force on the  
38 unconstrained atoms was less than 0.03 eV Å<sup>-1</sup>. Two 6MP radicals (without the H atom on the  
39  
40  
41  
42  
43  
44  
45  
46  
47  
48  
49  
50  
51  
52  
53  
54  
55  
56  
57  
58  
59  
60

1  
2  
3 –SH group) per unit cell are placed just on one side of the slab and all calculations include a  
4  
5 dipole correction. Radical 6MP species were optimized in an asymmetric box of  $20 \text{ \AA} \times 20 \text{ \AA} \times$   
6  
7  $40 \text{ \AA}$ .  
8  
9

## 10 11 12 13 14 15 **RESULTS AND DISCUSSION**

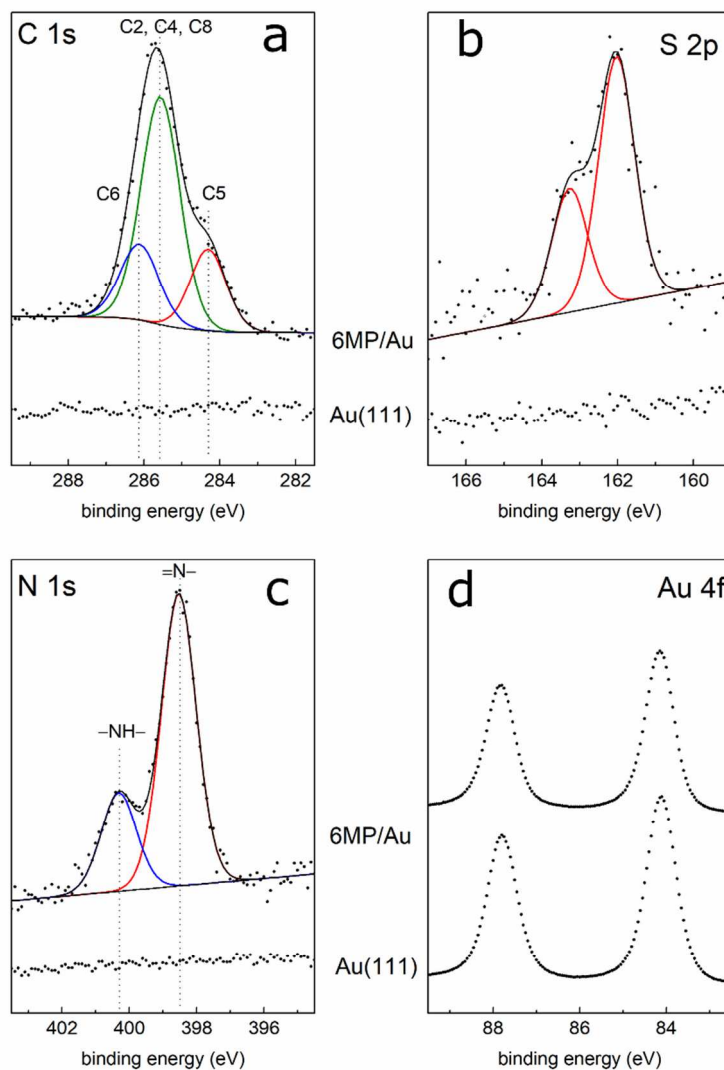
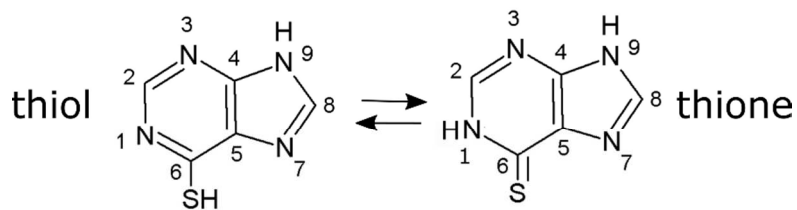
16  
17  
18 Figure 1a-d shows the C 1s, N 1s, S 2p and Au 4f XPS spectra corresponding to the initial  
19  
20 Au(111) surface (bottom spectra) and the 6MP modified surface (top spectra). Initially there is  
21  
22 no C, S or N present on the surface and only Au related signals are observed. After formation of  
23  
24 the 6MP self-assembled monolayer XPS shows the expected presence of C, N and S on the  
25  
26 surface as well as the attenuation of the Au signal. The corrected XPS C:N:S ratio is 5.3:4.1:1  
27  
28 which is in very good agreement with the expected 5:4:1 stoichiometric ratio (see Figure 1 top).  
29  
30 The C 1s spectrum shown in Figure 1a could be fitted with three components positioned at 284.2,  
31  
32 285.5 and 286.0 eV. The relative area of the peaks is 1:3:1 in excellent agreement with the  
33  
34 assignment of Boland et al.:<sup>7</sup> the 284.2 eV component is due to C5, the 285.5 eV component is  
35  
36 due to C2, C4 and C8 and the 286 eV component is due to C6.<sup>7,21</sup> The S 2p XPS region  
37  
38 corresponding to the 6MP SAM displayed in Figure 1b shows the characteristic doublet with the  
39  
40 S  $2p_{3/2}$  at  $\sim 162$  eV and the S  $2p_{1/2}$  at 163.3 eV with the expected 2:1 intensity ratio.<sup>22</sup> The  
41  
42 binding energy values indicate formation of thiolate S–Au bonds and the absence of thione or  
43  
44 thiol groups on the surface,<sup>23</sup> i.e. all S atoms on the molecule form a thiolate bond with Au.  
45  
46  
47  
48  
49  
50

51 The N 1s spectrum of 6MP SAMs requires further considerations. 6MP has several possible  
52  
53 thione (S=C–)/thiol (HS–C–) tautomeric configurations that differ in the number of iminic (=N–)  
54  
55 and aminic (–NH–) nitrogens.<sup>24,25</sup> In the thione tautomer the molecules have two aminic and two  
56  
57  
58  
59  
60



1  
2  
3 iminic nitrogens, whereas in the thiol tautomer the molecules have one aminic and three iminic  
4 nitrogens (Figure 1 top). Consequently, the N 1s XPS spectrum shown in Figure 1c contains two  
5  
6 contributions: the low binding energy component at 398.4 eV is due to iminic nitrogens whereas  
7  
8 the high binding energy component at 400.2 eV is due to aminic nitrogens.<sup>26</sup> In agreement with  
9  
10 Boland et al.<sup>7</sup> we observe a 3:1 ratio between the iminic and aminic N components. This  
11  
12 suggests that the molecule is adsorbed in the thiol form with 3 iminic and 1 aminic nitrogens.  
13  
14 Our DFT calculations indicates that one of the iminic nitrogens interacts with Au, however we  
15  
16 do not expect this interaction to shift the N 1s binding energy position as SAMs with amine head  
17  
18 and anchor groups have very similar N 1s binding energies.<sup>27-29</sup> Thus our XPS measurements  
19  
20 suggest that the molecule binds in the thiol form, with three iminic nitrogens and one aminic  
21  
22 nitrogen ruling out the possible mixture of tautomers in the 6MP SAM under the conditions we  
23  
24 employed for the formation of the monolayer.  
25  
26  
27  
28  
29  
30

31  
32 The Au 4f spectra in Figure 1d show the characteristic Au 4f<sub>7/2</sub> (84.0 eV) and Au 4f<sub>5/2</sub> (87.7  
33  
34 eV) doublet with a 4:3 intensity ratio. The thickness (d) of the 6MP self-assembled monolayer  
35  
36 can be estimated using the following equation:  $I = I_0 \exp(-d / \lambda \cos\theta)$ , where I is the substrate  
37  
38 intensity of the SAM-covered surface and I<sub>0</sub> is that of the bare substrate,  $\theta$  is the angle of  
39  
40 detection with respect to the surface normal and  $\lambda$  is the photoelectron attenuation length ( $\lambda$  is  
41  
42 equal to 42 Å for electrons with 1402 eV kinetic energy and self-assembled alkane chains).<sup>30</sup> The  
43  
44 estimated thickness is approximately 0.6 nm suggesting a monolayer of upright standing  
45  
46 molecules. Finally we can use the S:Au ratio to estimate the molecular coverage in the SAM.<sup>6</sup>  
47  
48 This yields a coverage of 0.25 6MP molecules per Au surface atom ( $3.5 \times 10^{14}$  molecules cm<sup>-2</sup>)  
49  
50 in excellent agreement with estimations based on the electrochemical reductive desorption of  
51  
52 6MP SAMs on Au(111).<sup>6</sup>  
53  
54  
55  
56  
57  
58  
59  
60



47  
48  
49  
50  
51  
52  
53  
54  
55  
56  
57  
58  
59  
60

**Figure 1.** XPS spectra of the initial and of the 6MP modified Au(111) surface: (a) C1s, (b) S 2p, (c) N 1s and (d) Au 4f. Top: thiol and thione 6MP tautomers.

1  
2  
3 The adsorption geometry of 6MP over Au(111) was determined using near edge X-ray  
4 absorption fine structure spectroscopy (NEXAFS). Figure 2a shows the adsorption step-edge  
5 normalized N K-edge NEXAFS spectra measured at 90°, 70°, 50° and 30° photon incidence  
6 angle with respect to the sample surface. The spectra display two main resonances: a N 1s to  $\pi^*$   
7 transition at 398.7 eV<sup>31</sup> and a N 1s to  $\sigma^*$  transition at 407.1 eV.<sup>12</sup> Note that the  $\pi^*$  resonance is  
8 attenuated probably due to intermolecular interactions or interactions with the substrate.<sup>32,33</sup> The  
9 N 1s to  $\pi^*$  transition is larger for normal incidence whereas the N 1s to  $\sigma^*$  transition is larger for  
10 grazing incidence. The observed normalized transition intensity dependence with photon  
11 incidence angle ( $\theta$ ) shown in Figure 2b indicates a tilted molecular plane in line with the dipole  
12 selection rules.<sup>15</sup> Figure 2b also shows the calculated normalized  $\pi^*$  curves for different angles  
13 between the vector  $\pi^*$  orbital and the surface normal ( $\alpha$ ).<sup>15</sup> Comparison of the experimental and  
14 calculated intensities as a function of photon incidence angle indicates a tilt angle between the  
15 molecular plane and the surface of 61° in line with the proposed vertical adsorption geometry on  
16 Au surfaces.<sup>13</sup>  
17  
18  
19  
20  
21  
22  
23  
24  
25  
26  
27  
28  
29  
30  
31  
32  
33  
34  
35  
36  
37  
38  
39  
40  
41  
42  
43  
44  
45  
46  
47  
48  
49  
50  
51  
52  
53  
54  
55  
56  
57  
58  
59  
60

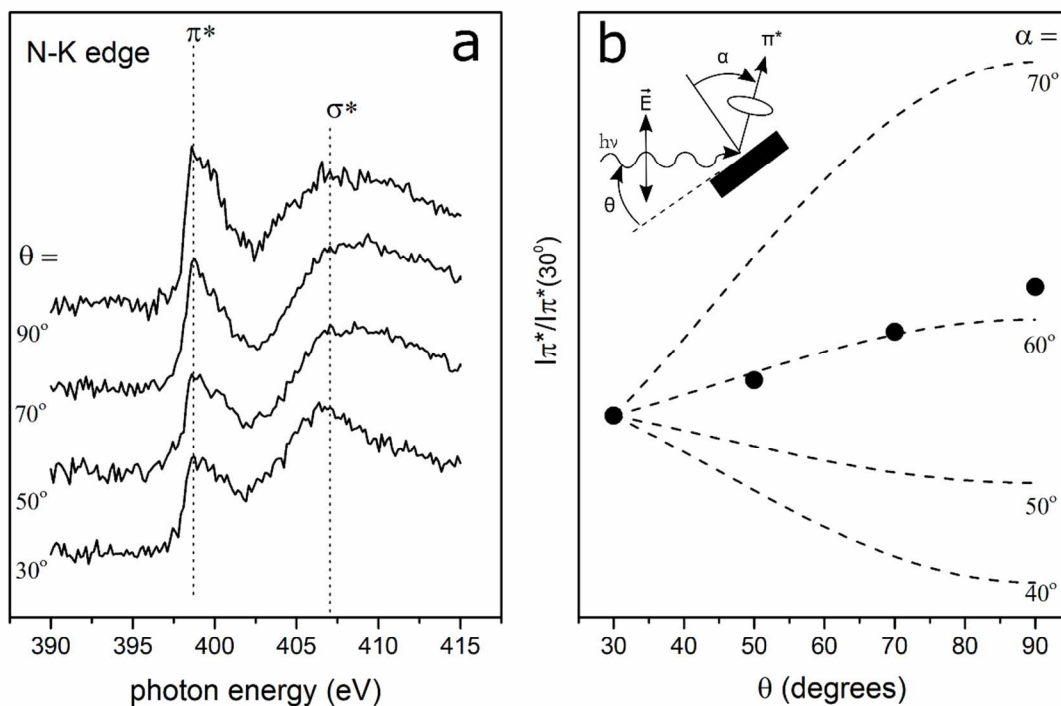


**Figure 2.** (a) N K-edge NEXAFS spectra taken from 6MP self-assembled monolayer on Au(111) as a function of photon incidence angle. (b) Normalized N 1s to  $\pi^*$  transition intensity as a function of photon incidence angle. Also shown are the theoretical curves corresponding to a  $\pi$  system on a threefold symmetry substrate (dashed lines).

The electronic structure of the 6MP SAM on Au(111) was studied using UPS. Figure 3 shows the UPS spectra corresponding to the bare Au(111) surface (red curve) and to the 6MP SAM on Au(111) (black). Figure 3a shows the secondary electron cut-off and Figure 3b shows the occupied density of states below the Fermi Edge. The UPS spectrum corresponding to the Au(111) surface shows the well-known electronic structure with a broad and flat 6s band below the Fermi edge and the intense 5d band showing one of the peaks at 2.84 eV.<sup>34</sup> From the width

(W) of the UPS spectrum we can calculate the work function ( $\Phi$ ) of our Au(111) substrate:  $\Phi = 21.21 \text{ eV} - W = 5.35 \text{ eV}$  which is in excellent agreement with values reported for this crystalline surface.<sup>35</sup>

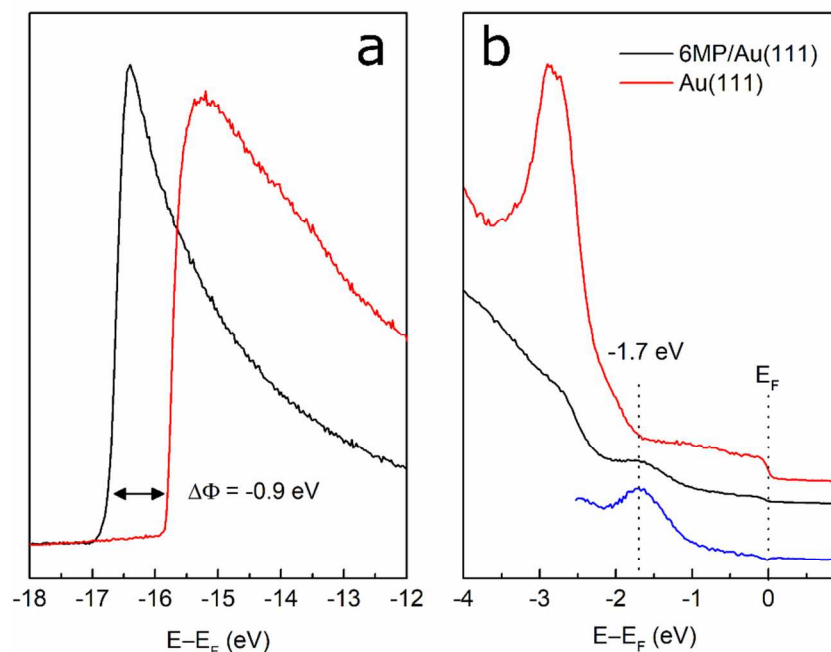


**Figure 3.** UPS spectra of the bare Au(111) substrate (red) and 6MP SAM on Au(111) (black). (a) shows work function changes ( $\Delta\Phi$ ) calculated from the secondary electron cut-off and (b) shows the occupied states. Molecular states are highlighted in the 6MP/Au(111) minus Au(111) blue spectrum.

The secondary electron cut-off shift observed in Figure 3a implies that formation of the 6MP self-assembled monolayer decreases the work function of Au(111) by -0.9 eV in agreement with the DFT calculations discussed below. Thus, 6MP molecules form a dipole layer with negative charges at the SAM/metal interface and positive at the vacuum/SAM interface.<sup>36,37</sup> We

1  
2  
3 estimated a component of the molecular dipole perpendicular to the surface<sup>38</sup> equal to 1.05 D  
4  
5 from the work function change, using a surface density of 3.47 nm<sup>-2</sup> and a relative dielectric  
6  
7 constant of the SAM equal to 1.5.<sup>39</sup>  
8  
9

10  
11 When the 6MP monolayer is present on the Au(111) surface the Au 5d and 6s bands decrease  
12  
13 in intensity as the adsorbate attenuates the photoelectrons. Moreover, a new electronic state is  
14  
15 observed at -1.7 eV below the Fermi edge which can be clearly seen when the Au(111) spectrum  
16  
17 is subtracted from the 6MP spectrum (blue curve). No electronic states are typically observed in  
18  
19 the region up to -1.5 eV below the Fermi edge in the UPS spectra of C<sub>2</sub>-C<sub>18</sub> alkanethiol self-  
20  
21 assembled monolayers.<sup>34,40,41</sup> However, Alloway *et al* found a very weak UPS band at -1.4 eV  
22  
23 after formation of a C<sub>3</sub> alkanethiol SAM on Au(111). This state was attributed to ionization of  
24  
25 the S-Au orbital.<sup>42</sup> Furthermore, benzenethiol SAMs on Au(111) also show a very weak UPS  
26  
27 band at -1.4 eV attributed to photoemission from a S-Au orbital.<sup>43</sup> In line with the above, our  
28  
29 DFT calculations discussed below indicate that 6MP on Au(111) has a very weak electronic state  
30  
31 at round -1.2 eV below the Fermi level which is due to the S-Au bond. Thus the newly  
32  
33 observed electronic state for 6MP on Au(111) at -1.7 eV cannot be attributed to photoemission  
34  
35 from the S-Au orbital.  
36  
37  
38  
39  
40  
41  
42  
43  
44  
45  
46  
47  
48  
49  
50  
51  
52  
53  
54  
55  
56  
57  
58  
59  
60

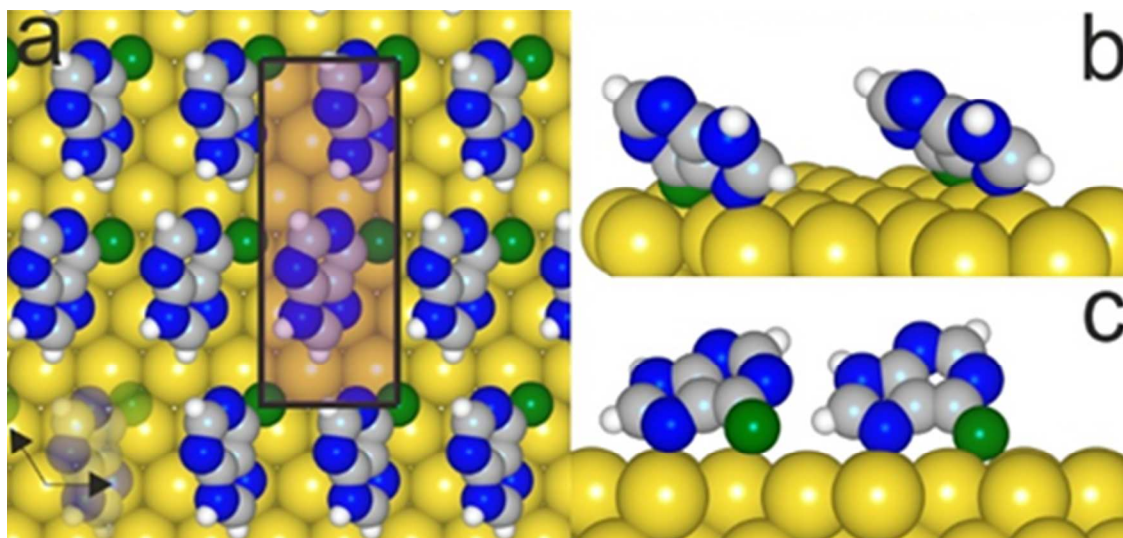
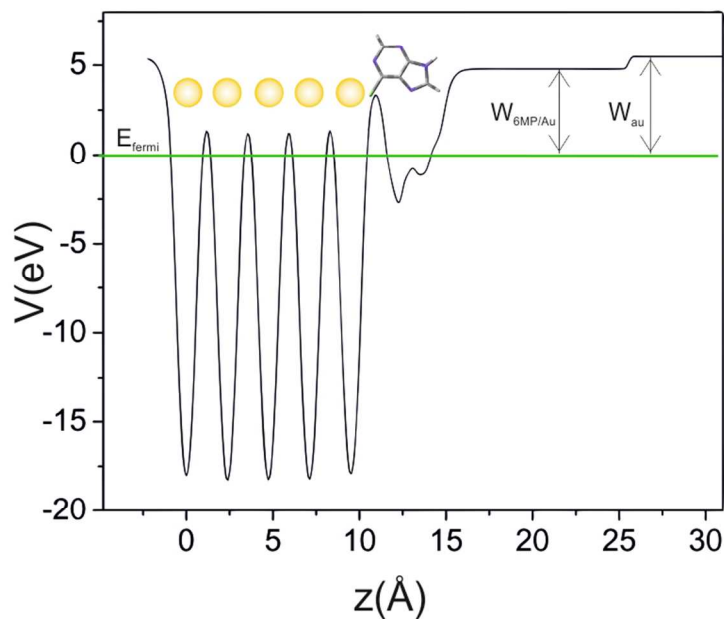


**Figure 4.** Optimized structure of the  $\begin{pmatrix} 2 & 0 \\ 3 & 6 \end{pmatrix}$  lattice on the unreconstructed Au(111) surface with two 6MP molecules per unit cell: (a) top view; (b) and (c) lateral view. Color of the atoms: yellow, Au; green, S; gray, C; blue: N; white, H. The unit cell is outlined.

Density functional theory (DFT) calculations were carried out to analyze the electronic properties of the 6MP self-assembled monolayer on Au(111) and to gain molecular insight into the experimental results. The surface structure was modeled with a  $\begin{pmatrix} 2 & 0 \\ 3 & 6 \end{pmatrix}$  unit cell,  $(2 \times 3\sqrt{3})$  in Wood notation, based on the short range ordered structure observed in the STM results discussed below (see Figure 8). The optimized structure is presented in Figure 4. It contains two 6MP moieties per unit cell, which corresponds to a surface coverage of 0.17 per unit cell ( $2.2 \times 10^{14}$  molecules  $\text{cm}^{-2}$ ). For this coverage, we found that each 6MP molecular plane in the unit cell is tilted  $34.8^\circ$  and  $27.4^\circ$  with respect to the Au surface, i.e. a lower tilt angle than the estimated by NEXAFS ( $61^\circ$ ). A likely reason for this discrepancy will be presented below when discussing the STM results. The total thickness of the SAM resulting from the structure relaxation is nearly 0.3 nm, i.e. smaller

1  
2  
3 than the calculated from XPS measurements (0.6 nm). This difference will also be discussed  
4  
5 below. The optimized molecular structure calculated with DFT involves a thiolate (S–Au) bond  
6  
7 and a bond between an iminic nitrogen (=N7–) and a Au surface atom in line with the XPS  
8  
9 observed 3:1 iminic:aminic ratio which rules out other adsorbed thione tautomers.  
10  
11

12  
13 The difference between the DFT calculated potential in the vacuum region and the Fermi level  
14  
15 can be used to estimate the work function.<sup>35</sup> Indeed, our DFT calculations yield a Au(111) work  
16  
17 function of 5.4 eV in excellent accord with our UPS measurement (5.35 eV). Formation of the  
18  
19 6MP SAM changes the potential in the direction perpendicular to the surface yielding a work  
20  
21 function value of 4.7 eV (Figure 5).  
22  
23  
24  
25  
26  
27



28  
29  
30  
31  
32  
33  
34  
35  
36  
37  
38  
39  
40  
41  
42  
43  
44  
45  
46  
47  
48  
49  
50 **Figure 5.** Plane averaged electrostatic potential of a slab comprising five layers of Au atoms and  
51  
52 one layer of 6MP. The Fermi energy level ( $E_F = 0$ ) is indicated by a green line. The work  
53  
54 function of the clean and the adsorbed surfaces are indicated with respect to the  $E_F$ .  
55  
56  
57  
58  
59  
60



Therefore, the shift with respect to the clean surface is -0.7 eV. This result is in good agreement with the shift obtained from our UPS data (-0.9 eV). The smaller shift found in the calculations, by about -0.2 eV, may be related to the fact that the surface coverage modeled with DFT was 30% smaller than in the experimental measurements. As discussed above, from the estimated work function change we can calculate the component of the molecular dipole perpendicular to the surface resulting in a value equal to  $\mu_{\perp} = 1.12$  D.

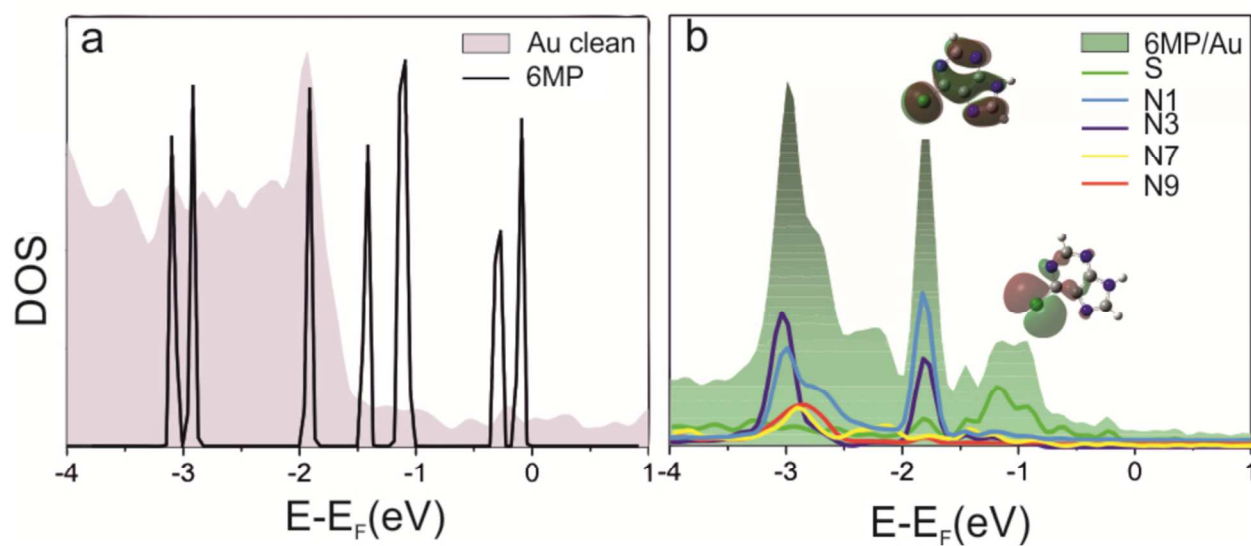


**Figure 6.** (a) Total density of states of Au(111) surface and 6MP molecule gas phase (the energy level of the HOMO is set at 0 eV). (b) 6MP adsorbed on Au(111). Projected density of states on the S and N atoms are shown in different colours.

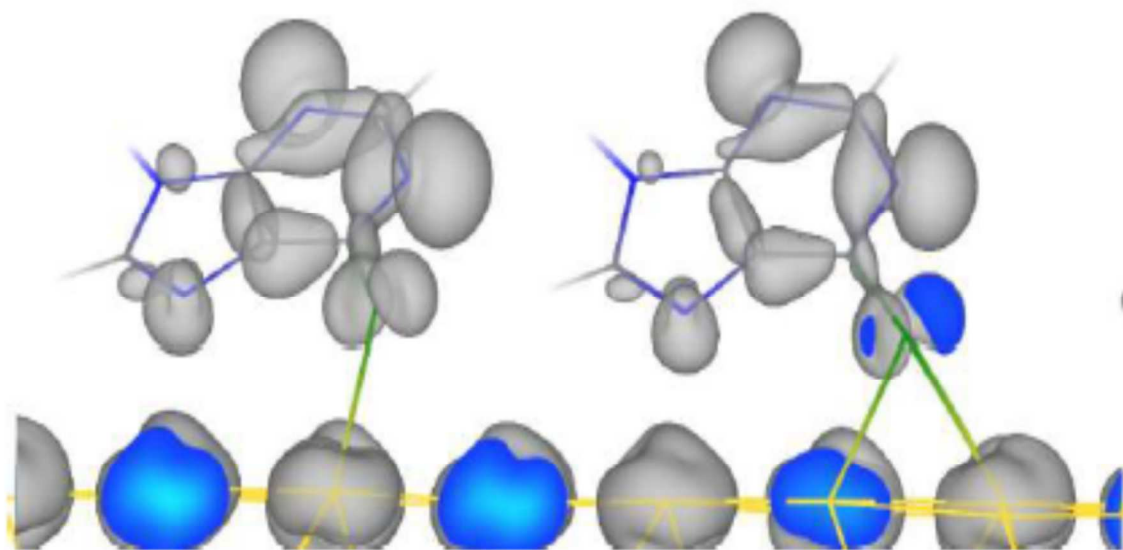
Figure 6a depicts the total density of states (DOS) for the clean Au(111) surface and the DOS of 6MP molecules in the gas phase (in this case the energy level of the HOMO (highest orbital

1  
2  
3 molecular orbital) is set at 0 eV). The main features observed in the clean Au(111) DOS are a  
4 broad and flat signal below the Fermi edge that corresponds to the 6s band followed by a sharper  
5 signal which corresponds to the 5d states. These features are in general agreement with the UPS  
6 spectrum of the clean surface presented in Figure 3. Figure 6b shows the total density of states  
7 after formation of the 6MP SAM over Au(111). Projected density of states on the S and N atoms  
8 are shown using different colors.  
9

10  
11  
12 We also analyzed the electronic structure of the 6MP radical in the gas phase. DFT does not  
13 yield the correct HOMO–LUMO gap (it is underestimated) nor the precise HOMO and LUMO  
14 energy location with respect to the Fermi level. However, major trends can be discussed using  
15 the shape of the frontier orbitals. After adsorption of 6MP on the Au(111) surface the electronic  
16 states can be stabilized and shifted to lower energies. Keep in mind that after breaking the S–H  
17 bond the highest molecular orbital is single occupied (SOMO) and can accept charge from the  
18 Au surface. We have determined the surface plots of the 6MP radical frontier orbitals (insets in  
19 Figure 6b). The highest charge density in this orbital is on the S atom and has the correct shape  
20 to interact with the broad Au s band giving a hybridized electronic state at around -1.2 eV below  
21 the Fermi level. This fact is in excellent agreement with previous UPS measurements of alkyl  
22 and aromatic thiol SAMs.<sup>42–44</sup> Here we should note that this band is too weak to be observed in  
23 our UPS spectrum.  
24  
25  
26  
27  
28  
29  
30  
31  
32  
33  
34  
35  
36  
37  
38  
39  
40  
41  
42  
43  
44  
45

46 It is also clear in Figure 6b that a new sharp band appears at around -1.7 eV in excellent  
47 agreement with the UPS spectrum shown in Figure 3. Its narrow shape suggests a strongly  
48 localized state. This state can be correlated with the HOMO-1 state of the 6MP radical which  
49 has a charge density of  $\pi$  character and is delocalized in the bicyclic system. The projected DOS  
50  
51  
52  
53  
54  
55  
56  
57  
58  
59  
60

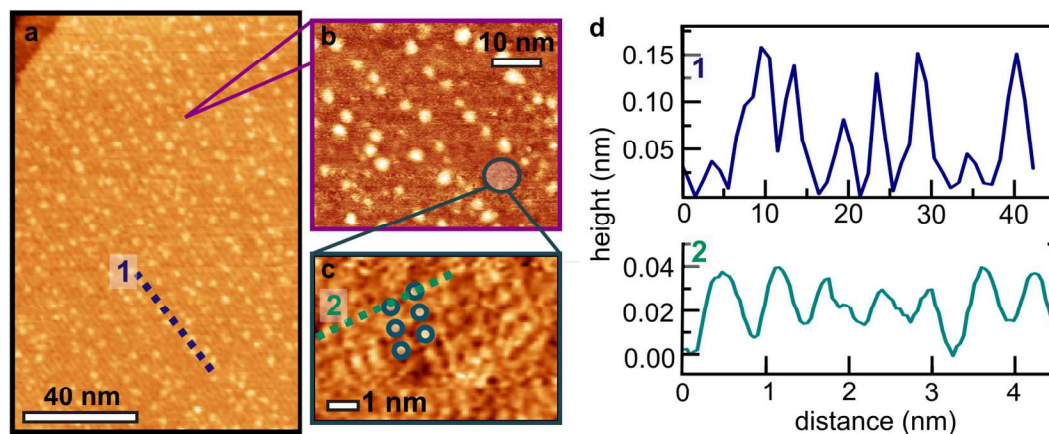
1  
2  
3 shows that the major electronic contribution to this band comes from the pyrimidine ring. This is  
4 clearly seen in Figure 7 which shows the density of states integrated between -1.6 and -2 eV with  
5 larger charge densities in the pyrimidine ring N1 and N3 nitrogens. On the other hand, the  
6 larger charge densities in the pyrimidine ring N1 and N3 nitrogens. On the other hand, the  
7 iminic nitrogen involved in the N–Au bond (N7) is strongly stabilized at -3 eV and is hybridized  
8 with the Au 5d band. Finally, we expect a weak electronic coupling of the  $\pi$  electrons of the  
9 6MP aromatic structure to the metal substrate due to its adsorption geometry.  
10  
11  
12  
13  
14  
15  
16  
17  
18  
19  
20  
21  
22  
23  
24  
25  
26  
27  
28  
29  
30  
31  
32  
33  
34  
35  
36  
37  
38  
39  
40



41 **Figure 7.** Charge density isosurfaces integrated between -1.6 and -2 eV for both 6MP molecules  
42 in the unit cell tilted  $34.8^\circ$  and  $27.4^\circ$  with respect to the Au surface.  
43  
44  
45  
46  
47  
48  
49

50 The electronic structure of the 6MP monolayer on Au(111) calculated with DFT agrees very well  
51 with that measured experimentally both in terms of the dipole layer formed and the valence band  
52 structure. Furthermore, the molecular structure calculated with DFT is in line with the  
53  
54  
55  
56  
57  
58  
59  
60

1  
2  
3 photoemission data predicting a thiolate bond and an iminic nitrogen bond with the Au(111)  
4 surface. However, DFT predicts an average tilt angle of  $31.1^\circ$  between the molecular plane and  
5 the Au surface whereas NEXAFS estimates a  $60^\circ$  tilt angle. In order to understand this  
6 discrepancy we carry out STM measurements of the 6MP SAM on Au(111).  
7  
8  
9  
10  
11  
12  
13



14  
15  
16  
17  
18  
19  
20  
21  
22  
23  
24  
25  
26  
27  
28  
29  
30  
31 **Figure 8.** (a) STM image corresponding to 6MP SAM on Au(111). (b-c) Zoom-in of image a,  
32 showing the two 6MP structures on the surface: (b) agglomerates and (c) 2D lattice. Molecule  
33 position in the lattice are indicated as blue dots. (d) Cross sections of the lines 1 and 2 indicated  
34 in the images.  
35  
36  
37  
38  
39  
40  
41  
42  
43

44  
45 Figure 8a shows a large area STM image corresponding to a 6MP self-assembled monolayer on  
46 Au(111). The surface coverage is 0.25 6MP molecules per Au surface atom, i.e. the same  
47 coverage employed in the photoemission experiments discussed above. Smaller size images  
48 (Figure 8b-c) reveal that there are two distinctive regions on the surface: aligned bright spots  
49 (islands) coexisting with short range well-ordered molecular structures. Figure 8c shows the  
50 short range well-ordered rectangular lattice present in the regions not covered by the aligned  
51  
52  
53  
54  
55  
56  
57  
58  
59  
60

1  
2  
3 6MP islands. The lattice has a  $\begin{pmatrix} 2 & 0 \\ 3 & 6 \end{pmatrix}$  structure as previously determined.<sup>6,9</sup> Line cross sections  
4  
5  
6 of the aligned 6MP islands shown in Figure 8a and the well-ordered molecular structures shown  
7  
8 in Figure 8c indicate that the apparent height of the former is at least three times as large. Given  
9  
10 that our DFT calculations indicate that the 6MP molecules form an average angle of 31.1° with  
11  
12 respect to the surface in the well-ordered molecular structures, the larger apparent height of the  
13  
14 aligned islands suggest that they are composed of standing upright 6MP molecules which are  
15  
16 presumably interacting via  $\pi$ - $\pi$  stacking. Note that the higher 6MP islands could be interacting  
17  
18 with Au adatoms. Recall that in our DFT model the 6MP surface coverage is around 30%  
19  
20 smaller than the experimental surface coverage. In a denser monolayer, the  $\pi$  molecular rings  
21  
22 would tend to stand upright in order to accommodate more molecules. Note that the transition  
23  
24 from flat lying to upright standing that takes place while increasing the molecular coverage has  
25  
26 been observed for other aromatic molecules.<sup>45</sup> Thus, the molecular aggregates observed with  
27  
28 STM account for the different tilt angle estimations obtained from NEXAFS measurements and  
29  
30 DFT calculations. NEXAFS suggests a larger tilt angle as we observe the average between the  
31  
32 standing upright molecules in the islands and the flatter molecules in the well-ordered structures.  
33  
34 Consequently, the experimentally estimated monolayer thickness is larger than the DFT  
35  
36 calculated thickness.  
37  
38  
39  
40  
41  
42  
43  
44  
45  
46

## 47 CONCLUSIONS

48  
49  
50 Photoemission measurements and DFT calculations show that 6MP molecules self-assemble on  
51  
52 Au(111) bonding to the substrate via S–Au thiolate and iminic N–Au bonds. The molecule  
53  
54 binds to the metal surface in the thiol form with three iminic and one aminic nitrogens. The  
55  
56  
57  
58  
59  
60

1  
2  
3 SAM forms a dipole layer with negative charges residing at the metal/monolayer interface and  
4 positive charges at the monolayer/vacuum interface. This results in a work function decrease of -  
5  
6 0.9/-0.7 eV with respect to that of clean Au(111) surface depending of surface coverage. DFT  
7  
8 calculations show that the S–Au bond has a weak band in the total density of states located -1.2  
9  
10 eV below the Fermi edge whereas the iminic nitrogen involved in bonding is stabilized at -3 eV  
11  
12 and is hybridized with the Au 5d band. Photoemission measurements show the presence of a  
13  
14 new electronic state located at -1.7 eV that corresponds to a  $\pi$  localized molecular state with  
15  
16 major electronic contributions in the pyrimidine ring. STM measurements show that dense 6MP  
17  
18 monolayers exhibit two molecular domains. The first one corresponds to short range well-  
19  
20 ordered molecular structures where DFT estimates a  $31^\circ$  average angle between the 6MP  
21  
22 molecular plane and the surface plane. Whereas, the second domain consists of aligned 6MP  
23  
24 islands. Height profiles suggest that 6MP molecules in the latter domain are upright standing  
25  
26 presumably interacting via  $\pi$ – $\pi$  stacking. The coexistence of both molecular structures is in  
27  
28 agreement with the  $61^\circ$  adsorption angle between the molecular plane and the substrate estimated  
29  
30 from the NEXAFS measurements. Our results provide new physical insight into the molecular  
31  
32 and electronic structure of self-assembled monolayers bound to gold surfaces with two surface  
33  
34 anchors.  
35  
36  
37  
38  
39  
40  
41  
42  
43  
44  
45

## 46 **ACKNOWLEDGMENTS**

47  
48 PC acknowledges MINECO (ENE2016-74889-C4-2-R, AEI-FEDER-UE) and also thankfully  
49  
50 acknowledges the computer resources provided by the Computer Support Service for Research  
51  
52 (SAII) at La Laguna University. RCS thanks ANPCyT for financial support (PICT 2016-0679).  
53  
54  
55  
56  
57  
58  
59  
60

1  
2  
3 CCF and FJW acknowledge financial support from CONICET. We acknowledge financial  
4 support from the Brazilian Synchrotron Light Laboratory LNLS to use the PGM beamline.  
5  
6  
7  
8  
9

## 10 REFERENCES

- 11  
12  
13 (1) Elion, G. The Purine Path to Chemotherapy. *Science* (80). **1989**, *244* (4900), 41–47.  
14  
15  
16 (2) Karran, P.; Attard, N. Thiopurines in Current Medical Practice: Molecular Mechanisms  
17 and Contributions to Therapy-Related Cancer. *Nat. Rev. Cancer* **2008**, *8* (1), 24–36.  
18  
19  
20  
21  
22 (3) Podsiadlo, P.; Sinani, V. A.; Bahng, J. H.; Kam, N. W. S.; Lee, J.; Kotov, N. A. Gold  
23 Nanoparticles Enhance the Anti-Leukemia Action of a 6-Mercaptopurine  
24 Chemotherapeutic Agent. *Langmuir* **2008**, *24* (2), 568–574.  
25  
26  
27  
28  
29  
30 (4) Ghorbani, M.; Hamishehkar, H.; Hajipour, H.; Arsalani, N.; Entezami, A. A. Ternary-  
31 Responsive Magnetic Nanocarriers for Targeted Delivery of Thiol-Containing Anticancer  
32 Drugs. *New J. Chem.* **2016**, *40* (4), 3561–3570.  
33  
34  
35  
36  
37  
38 (5) Wu, X.; Zhou, L.; Su, Y.; Dong, C.-M. Plasmonic, Targeted, and Dual Drugs-Loaded  
39 Polypeptide Composite Nanoparticles for Synergistic Cocktail Chemotherapy with  
40 Photothermal Therapy. *Biomacromolecules* **2016**, *17* (7), 2489–2501.  
41  
42  
43  
44  
45  
46 (6) Pensa, E.; Carro, P.; Rubert, A. A.; Benítez, G.; Vericat, C.; Salvarezza, R. C. Thiol with  
47 an Unusual Adsorption–Desorption Behavior: 6-Mercaptopurine on Au(111). *Langmuir*  
48 **2010**, *26* (22), 17068–17074.  
49  
50  
51  
52  
53  
54 (7) Boland, T.; Ratner, B. D. Two-Dimensional Assembly of Purines and Pyrimidines on  
55  
56  
57  
58  
59  
60

- 1  
2  
3 Au(111). *Langmuir* **1994**, *10* (10), 3845–3852.  
4  
5  
6  
7 (8) Carro, P.; Müller, K.; Maza, F. L.; Vericat, C.; Starke, U.; Kern, K.; Salvarezza, R. C.;  
8 Grumelli, D. 6-Mercaptopurine Self-Assembled Monolayers on Gold (001)-Hex:  
9 Revealing the Fate of Gold Adatoms. *J. Phys. Chem. C* **2017**, *121* (16), 8938–8943.  
10  
11  
12  
13  
14 (9) Lobo Maza, F.; Grumelli, D.; Carro, P.; Vericat, C.; Kern, K.; Salvarezza, R. C. The Role  
15 of the Crystalline Face in the Ordering of 6-Mercaptopurine Self-Assembled Monolayers  
16 on Gold. *Nanoscale* **2016**, *8* (39), 17231–17240.  
17  
18  
19  
20  
21  
22 (10) Bu, Y.; Huan, S.; Liu, X.; Shen, G.; Yu, R. Multiple-Angle-of-Incidence Polarization  
23 Infrared Reflection-Absorption Spectroscopy (MAI-PIRRAS) for Investigation of 6-  
24 Mercaptopurine SAMs on Smooth Silver Surface. *Vib. Spectrosc.* **2009**, *49* (1), 38–42.  
25  
26  
27  
28  
29  
30 (11) Chu, H.; Yang, H.; Huan, S.; Shen, G.; Yu, R. Orientation of 6-Mercaptopurine SAMs at  
31 the Silver Electrode as Studied by Raman Mapping and in Situ SERS. *J. Phys. Chem. B*  
32 **2006**, *110* (11), 5490–5497.  
33  
34  
35  
36  
37  
38 (12) Kim, K.; Han, Y.; Zhu, J.; Baik, J.; Shin, H.; Lee, H.; Kim, B. Purine on Graphene: PES  
39 and NEXAFS Study of a Heterocyclic Aromatic Organic Compound. *Curr. Appl. Phys.*  
40 **2016**, *16* (9), 1120–1123.  
41  
42  
43  
44  
45  
46 (13) Yang, H.; Liu, Y.; Liu, Z.; Yang, Y.; Jiang, J.; Zhang, Z.; Shen, G.; Yu, R. Raman  
47 Mapping and In Situ SERS Spectroelectrochemical Studies of 6-Mercaptopurine SAMs on  
48 the Gold Electrode. *J. Phys. Chem. B* **2005**, *109* (7), 2739–2744.  
49  
50  
51  
52  
53  
54 (14) Méndez De Leo, L. P.; de la Llave, E.; Scherlis, D.; Williams, F. J. Molecular and  
55  
56  
57  
58  
59  
60



- 1  
2  
3 Electronic Structure of Electroactive Self-Assembled Monolayers. *J. Chem. Phys.* **2013**,  
4 *138* (11), 114707.  
5  
6  
7  
8  
9 (15) Stöhr, J.; Outka, D. A. Determination of Molecular Orientations on Surfaces from the  
10 Angular Dependence of near-Edge X-Ray-Absorption Fine-Structure Spectra. *Phys. Rev.*  
11 *B* **1987**, *36* (15), 7891–7905.  
12  
13  
14  
15  
16 (16) Kresse, G.; Furthmüller, J. Efficiency of Ab-Initio Total Energy Calculations for Metals  
17 and Semiconductors Using a Plane-Wave Basis Set. *Comput. Mater. Sci.* **1996**, *6* (1), 15–  
18 50.  
19  
20  
21  
22  
23  
24 (17) Dion, M.; Rydberg, H.; Schröder, E.; Langreth, D. C.; Lundqvist, B. I. Van Der Waals  
25 Density Functional for General Geometries. *Phys. Rev. Lett.* **2004**, *92* (24), 246401.  
26  
27  
28  
29  
30 (18) Klimeš, J.; Bowler, D. R.; Michaelides, A. Chemical Accuracy for the van Der Waals  
31 Density Functional. *J. Phys. Condens. Matter* **2010**, *22* (2), 22201.  
32  
33  
34  
35  
36 (19) Blöchl, P. E. Projector Augmented-Wave Method. *Phys. Rev. B* **1994**, *50* (24), 17953–  
37 17979.  
38  
39  
40  
41 (20) Monkhorst, H. J.; Pack, J. D. Special Points for Brillouin-Zone Integrations. *Phys. Rev. B*  
42 **1976**, *13* (12), 5188–5192.  
43  
44  
45  
46  
47 (21) Avaldi, P. B. and P. O. and V. F. and O. P. and K. P. and M. C. and G. M. and A. A. B.  
48 and W. Z. and V. C. and Y. O. and L. Inner Shell Excitation, Ionization and  
49 Fragmentation of Pyrimidine. *J. Phys. Conf. Ser.* **2010**, *212* (1), 12002.  
50  
51  
52  
53  
54  
55 (22) Zharnikov, M. High-Resolution X-Ray Photoelectron Spectroscopy in Studies of Self-  
56  
57  
58  
59  
60

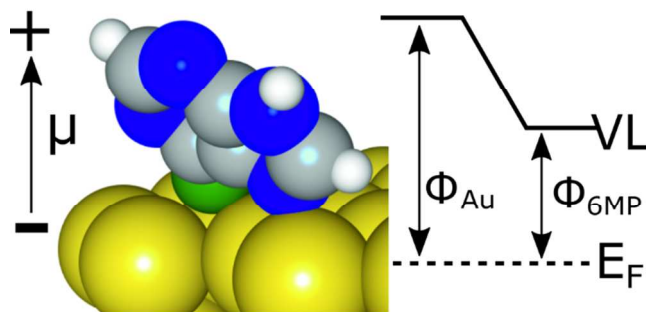
- 1  
2  
3 Assembled Organic Monolayers. *J. Electron Spectros. Relat. Phenomena* **2010**, 178–179,  
4  
5 380–393.  
6  
7  
8  
9 (23) Willey, T. M.; Vance, A. L.; van Buuren, T.; Bostedt, C.; Terminello, L. J.; Fadley, C. S.  
10  
11 Rapid Degradation of Alkanethiol-Based Self-Assembled Monolayers on Gold in  
12  
13 Ambient Laboratory Conditions. *Surf. Sci.* **2005**, 576 (1–3), 188–196.  
14  
15  
16  
17 (24) Viudez, A. J.; Madueño, R.; Pineda, T.; Blázquez, M. Stabilization of Gold Nanoparticles  
18  
19 by 6-Mercaptopurine Monolayers. Effects of the Solvent Properties. *J. Phys. Chem. B*  
20  
21 **2006**, 110 (36), 17840–17847.  
22  
23  
24  
25 (25) Pazderski, L.; Łakomska, I.; Wojtczak, A.; Szłyk, E.; Sitkowski, J.; Kozerski, L.;  
26  
27 Kamieński, B.; Koźmiński, W.; Tousek, J.; Marek, R. The Studies of Tautomerism in 6-  
28  
29 Mercaptopurine Derivatives by  $^1\text{H}$ – $^{13}\text{C}$ ,  $^1\text{H}$ – $^{15}\text{N}$  NMR and  $^{13}\text{C}$ ,  $^{15}\text{N}$  CPMAS-  
30  
31 Experimental and Quantum Chemical Approach. *J. Mol. Struct.* **2006**, 785 (1–3), 205–  
32  
33 215.  
34  
35  
36  
37 (26) Franke, M.; Marchini, F.; Steinrück, H.-P.; Lytken, O.; Williams, F. J. Surface Porphyrins  
38  
39 Metalate with Zn Ions from Solution. *J. Phys. Chem. Lett.* **2015**, 6 (23), 4845–4849.  
40  
41  
42  
43 (27) Dietrich, P. M.; Graf, N.; Gross, T.; Lippitz, A.; Krakert, S.; Schüpbach, B.; Terfort, A.;  
44  
45 Unger, W. E. S. Amine Species on Self-Assembled Monolayers of  $\omega$ -Aminothiulates on  
46  
47 Gold as Identified by XPS and NEXAFS Spectroscopy. *Surf. Interface Anal.* **2010**, 42 (6–  
48  
49 7), 1184–1187.  
50  
51  
52  
53 (28) Marmisollé, W. A.; Capdevila, D. A.; de la Llave, E.; Williams, F. J.; Murgida, D. H.  
54  
55 Self-Assembled Monolayers of  $\text{NH}_2$ -Terminated Thiulates: Order,  $P$  K a , and Specific  
56  
57  
58  
59  
60

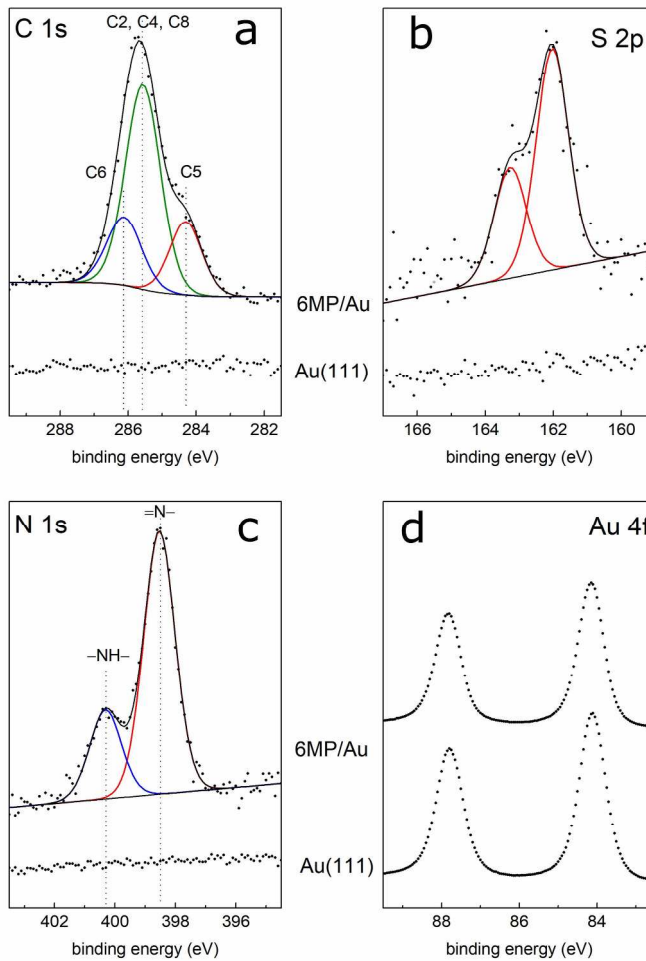
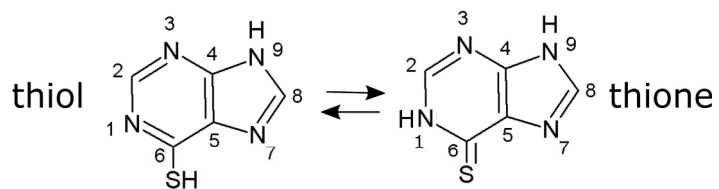
- 1  
2  
3 Adsorption. *Langmuir* **2013**, *29* (17), 5351–5359.
- 4  
5  
6 (29) de la Llave, E.; Clarenc, R.; Schiffrin, D. J.; Williams, F. J. Organization of Alkane  
7 Amines on a Gold Surface: Structure, Surface Dipole, and Electron Transfer. *J. Phys.*  
8 *Chem. C* **2014**, *118* (1), 468–475.
- 9  
10  
11  
12  
13  
14 (30) Laibinis, P. E.; Bain, C. D.; Whitesides, G. M. Attenuation of Photoelectrons in  
15 Monolayers of N-Alkanethiols Adsorbed on Copper, Silver, and Gold. *J. Phys. Chem.*  
16 **1991**, *95* (18), 7017–7021.
- 17  
18  
19  
20  
21  
22 (31) Lin, Y.-S.; Lin, H.-R.; Liu, W.-L.; Lee, Y. T.; Tseng, C.-M.; Ni, C.-K.; Liu, C.-L.; Tsai,  
23 C.-C.; Chen, J.-L.; Hu, W.-P. Measurement and Prediction of the NEXAFS Spectra of  
24 Pyrimidine and Purine and the Dissociation Following the Core Excitation. *Chem. Phys.*  
25 *Lett.* **2015**, *636*, 146–153.
- 26  
27  
28  
29  
30  
31  
32 (32) Zubavichus, Y.; Shaporenko, A.; Korolkov, V.; Grunze, M.; Zharnikov, M. X-Ray  
33 Absorption Spectroscopy of the Nucleotide Bases at the Carbon, Nitrogen, and Oxygen K-  
34 Edges. *J. Phys. Chem. B* **2008**, *112* (44), 13711–13716.
- 35  
36  
37  
38  
39  
40 (33) Tarek, A.; Swen, S.; A., E. D.; Martin, K.; Tobias, S.; Adrian, W.; Ryan, C.; Egbert, Z.;  
41 Andreas, T.; Michael, Z. The Effects of Embedded Dipoles in Aromatic Self-Assembled  
42 Monolayers. *Adv. Funct. Mater.* **2015**, *25* (25), 3943–3957.
- 43  
44  
45  
46  
47  
48 (34) Rieley, H.; Price, N. J.; White, R. G.; Blyth, R. I. R.; Robinson, a. W. A NEXAFS and  
49 UPS Study of Thiol Monolayers Self-Assembled on Gold. *Surf. Sci.* **1995**, *331–333*, 189–  
50  
51  
52  
53  
54  
55  
56  
57  
58  
59  
60

- 1  
2  
3 (35) De Renzi, V.; Rousseau, R.; Marchetto, D.; Biagi, R.; Scandolo, S.; del Pennino, U. Metal  
4 Work-Function Changes Induced by Organic Adsorbates: A Combined Experimental and  
5 Theoretical Study. *Phys. Rev. Lett.* **2005**, *95* (4), 46804.  
6  
7  
8  
9  
10  
11 (36) Reiss, H. The Fermi Level and the Redox Potential. *J. Phys. Chem.* **1985**, *89* (18), 3783–  
12 3791.  
13  
14  
15  
16 (37) Torasso, N.; Armaleo, J. M.; Tagliazucchi, M.; Williams, F. J. Simplified Approach to  
17 Work Function Modulation in Polyelectrolyte Multilayers. *Langmuir* **2017**, *33* (9), 2169–  
18 2176.  
19  
20  
21  
22  
23  
24 (38) Cahen, D.; Naaman, R.; Vager, Z. The Cooperative Molecular Field Effect. *Adv. Funct.*  
25 *Mater.* **2005**, *15* (10), 1571–1578.  
26  
27  
28  
29  
30 (39) Romaner, L.; Heimel, G.; Ambrosch-Draxl, C.; Zojer, E. The Dielectric Constant of Self-  
31 Assembled Monolayers. *Adv. Funct. Mater.* **2008**, *18* (24), 3999–4006.  
32  
33  
34  
35  
36 (40) Duwez, A.-S.; Pfister-Guillouzo, G.; Delhalle, J.; Riga, J. Probing Organization and  
37 Structural Characteristics of Alkanethiols Adsorbed on Gold and of Model Alkane  
38 Compounds through Their Valence Electronic Structure: An Ultraviolet Photoelectron  
39 Spectroscopy Study. *J. Phys. Chem. B* **2000**, *104* (38), 9029–9037.  
40  
41  
42  
43  
44  
45  
46 (41) Duwez, A.-S. Exploiting Electron Spectroscopies to Probe the Structure and Organization  
47 of Self-Assembled Monolayers: A Review. *J. Electron Spectros. Relat. Phenomena* **2004**,  
48 *134* (2–3), 97–138.  
49  
50  
51  
52  
53  
54 (42) Alloway, D. M.; Hofmann, M.; Smith, D. L.; Gruhn, N. E.; Graham, A. L.; Colorado, R.;  
55  
56  
57  
58  
59  
60

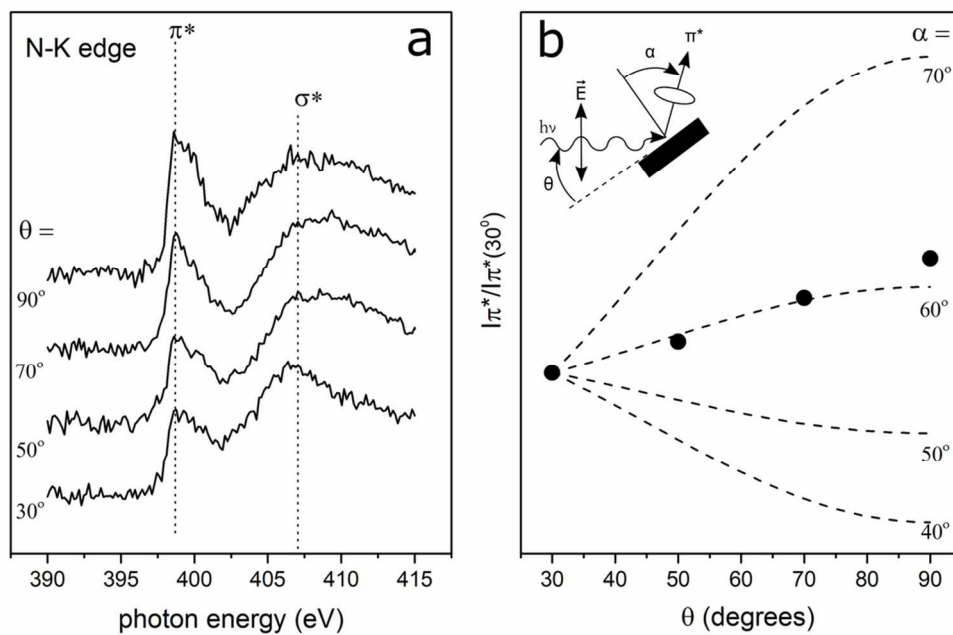
- 1  
2  
3 Wysocki, V. H.; Lee, T. R.; Lee, P. A.; Armstrong, N. R. Interface Dipoles Arising from  
4 Self-Assembled Monolayers on Gold : UV - Photoemission Studies of Alkanethiols and  
5 Partially Fluorinated Alkanethiols. *J. Phys. Chem. B* **2003**, *107*, 11690–11699.  
6  
7  
8  
9  
10  
11 (43) Whelan, C. M.; Barnes, C. J.; Walker, C. G. H.; Brown, N. M. D. Benzenethiol  
12 Adsorption on Au(111) Studied by Synchrotron ARUPS, HREELS and XPS. *Surf. Sci.*  
13 **1999**, *425* (2–3), 195–211.  
14  
15  
16  
17  
18 (44) Koslowski, B.; Tschetschetkin, A.; Maurer, N.; Ziemann, P. 4-Mercaptopyridine on  
19 Au(111): A Scanning Tunneling Microscopy and Spectroscopy Study. *Phys. Chem. Chem.*  
20 *Phys.* **2011**, *13* (9), 4045.  
21  
22  
23  
24  
25  
26 (45) Wechsler, D.; Fernández, C. C.; Steinrück, H.-P.; Lytken, O.; Williams, F. J. Covalent  
27 Anchoring and Interfacial Reactions of Adsorbed Porphyrins on Rutile TiO<sub>2</sub> (110). *J.*  
28 *Phys. Chem. C* **2018**, *122* (8), 4480–4487.  
29  
30  
31  
32  
33  
34  
35  
36  
37  
38  
39  
40  
41  
42  
43  
44  
45  
46  
47  
48  
49  
50  
51  
52  
53  
54  
55  
56  
57  
58  
59  
60

## TOC GRAPHIC



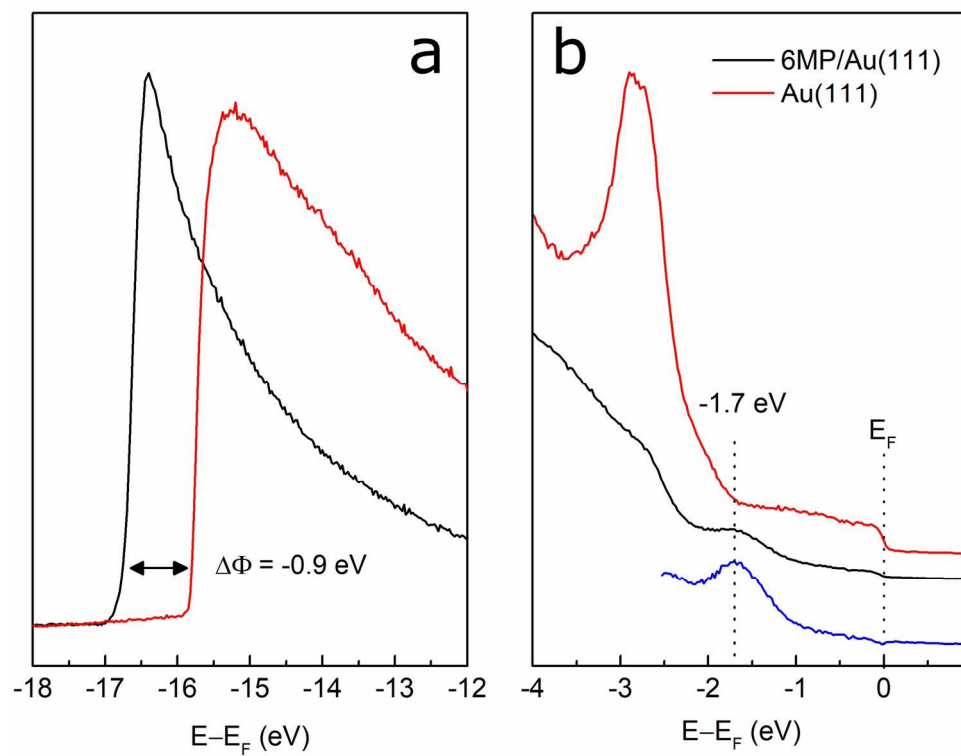


176x303mm (300 x 300 DPI)

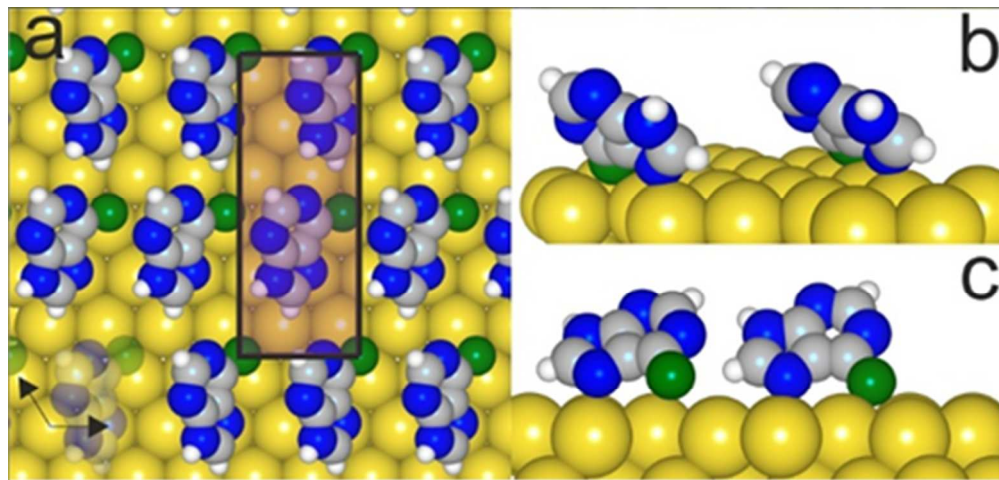


99x67mm (300 x 300 DPI)

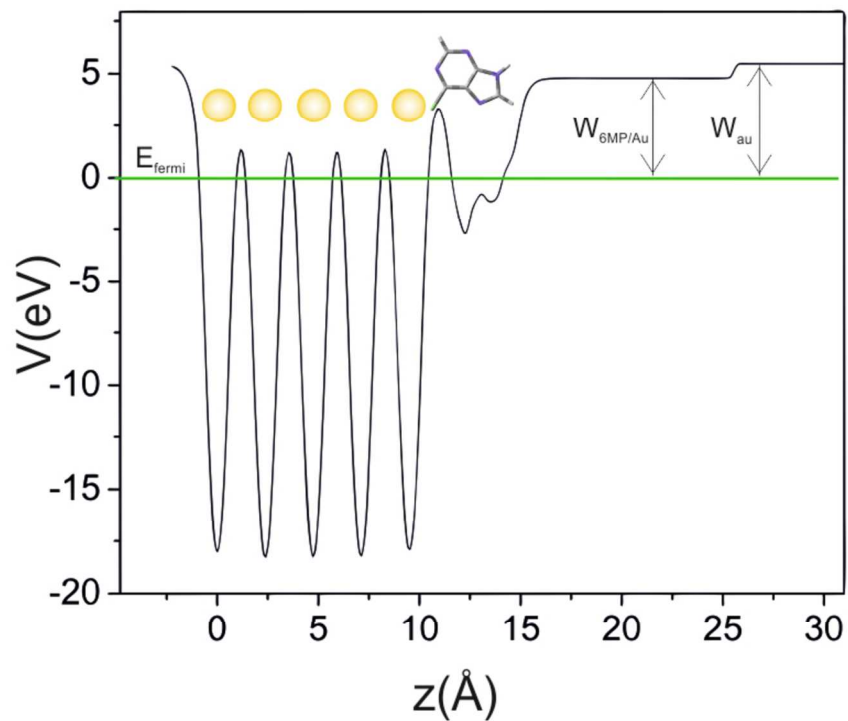




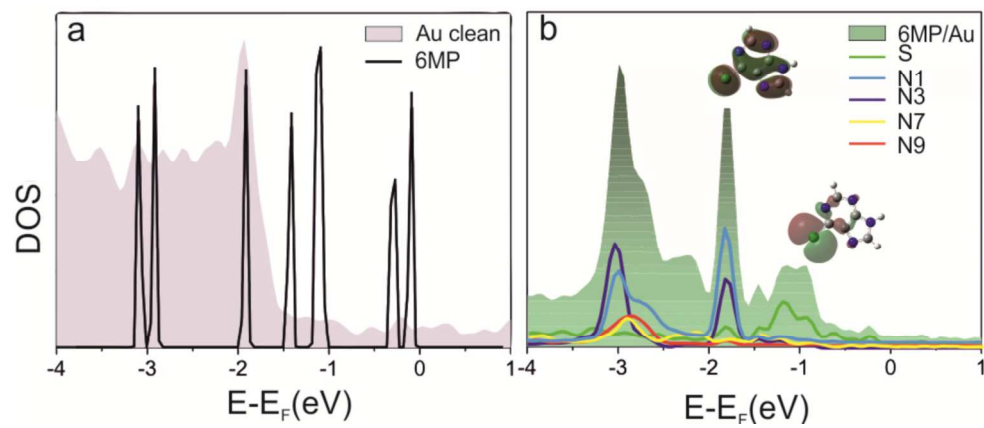
1  
2  
3  
4  
5  
6  
7  
8  
9  
10  
11  
12  
13  
14  
15  
16  
17  
18  
19  
20  
21  
22  
23  
24  
25  
26  
27  
28  
29  
30  
31  
32  
33  
34  
35  
36  
37  
38  
39  
40  
41  
42  
43  
44  
45  
46  
47  
48  
49  
50  
51  
52  
53  
54  
55  
56  
57  
58  
59  
60



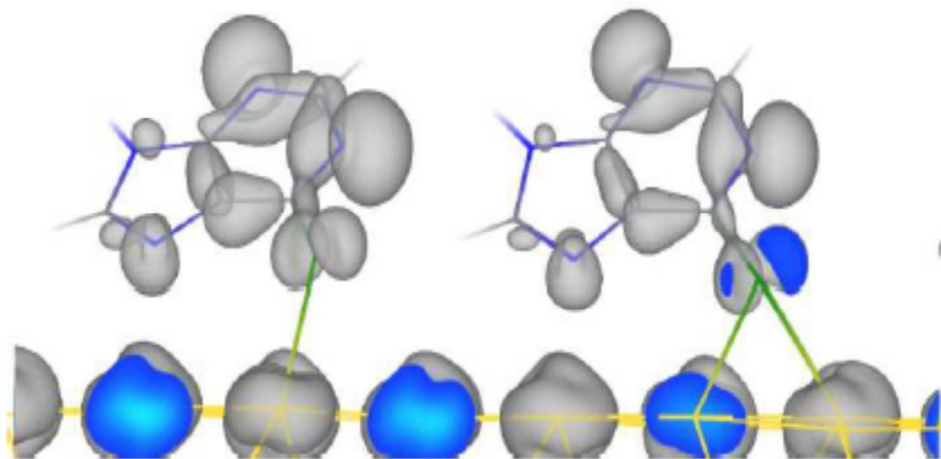
150x71mm (150 x 150 DPI)



120x97mm (300 x 300 DPI)

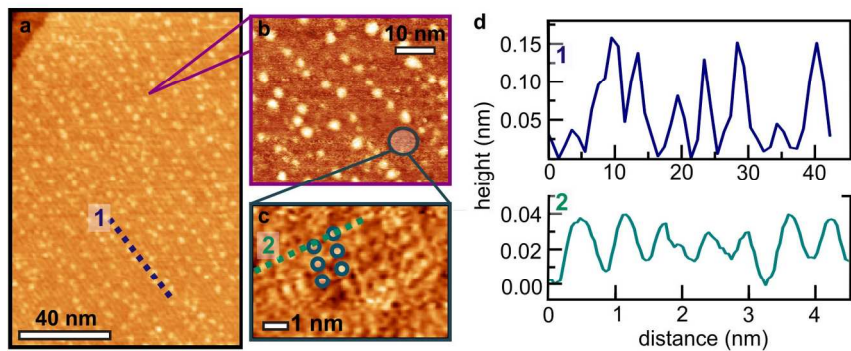


171x75mm (300 x 300 DPI)

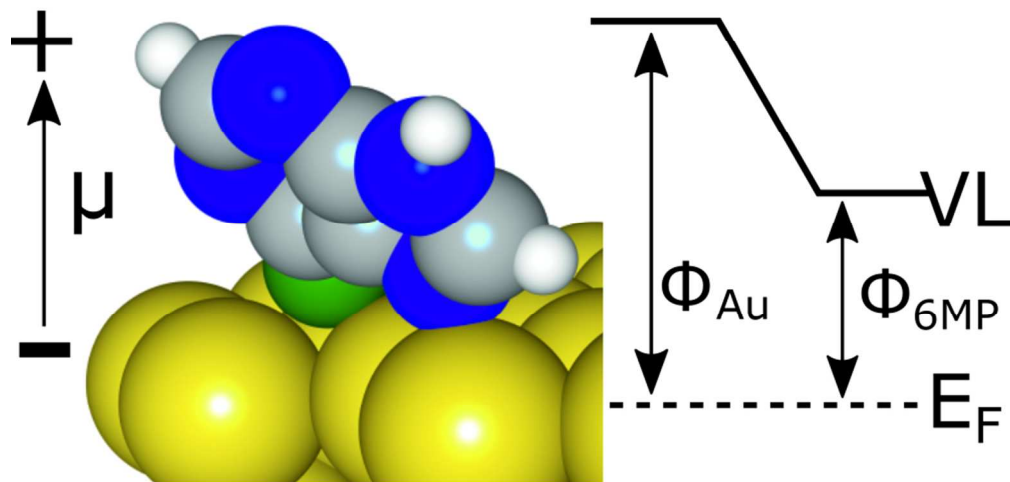


157x90mm (300 x 300 DPI)

1  
2  
3  
4  
5  
6  
7  
8  
9  
10  
11  
12  
13  
14  
15  
16  
17  
18  
19  
20  
21  
22  
23  
24  
25  
26  
27  
28  
29  
30  
31  
32  
33  
34  
35  
36  
37  
38  
39  
40  
41  
42  
43  
44  
45  
46  
47  
48  
49  
50  
51  
52  
53  
54  
55  
56  
57  
58  
59  
60



165x65mm (300 x 300 DPI)



84x45mm (300 x 300 DPI)